ADVANCED MATERIALS

DOI: 10.1002/adma.200800145

Direct Growth of Highly Mismatched Type II ZnO/ZnSe Core/Shell Nanowire Arrays on Transparent Conducting Oxide Substrates for Solar Cell Applications**

By *Kai Wang, Jiajun Chen, Weilie Zhou,* Yong Zhang,* Yanfa Yan, John Pern,* and *Angelo Mascarenhas*

A number of nanometer-scale photovoltaic (PV) concepts based on semiconductor nanowires have been developed or proposed in recent years, with either inorganic/organic hybrid[1–4] or all-inorganic approaches.[5–9] The quasi-one-dimensional (quasi-1D) structure is perhaps the optimized choice for optoelectronic devices such as solar cells and photodetectors, because it allows for maximal advantage to be taken of reduced dimensionality whilst retaining the last and only needed conduction channel. Besides the possibility of exploring quantum effects at the nanoscopic scale,[7,8] the quasi-1D system could be superior to the bulk material even at the mesoscopic scale, where the lateral size falls below the carrier diffusion length, for instance, by reducing the nonradiative recombination and carrier scattering loss[10,11] through elimination of the unnecessary lateral transport and the resulting recombination loss. Additionally, a nanowire array constitutes a natural architecture, such as a photonic crystal,[12] for light trapping.

The charge separation of the electron and hole is a key step in the generation of solar power in a PV device. In a conventional solar cell, it is typically achieved by a planar *p–n* homojunction along the path of the current flow or longitudinally. In nanometer-architecture PV devices, however, the charge separation is often facilitated by a type II or staggered energy alignment of a heterojunction, constructed from two materials for which both the valance and conduction bands of one component lie lower in energy than the corresponding bands of the other component. Such heterojunctions have been intensively investigated for solar cell applications, including dye-sensitized solar cells (DSSCs),[13] quantum-dot-sensitized solar cells (QDSSCs),[14,15] nanocrystal–polymer hybrids,[16] and bilayer nanocrystal films.[17] To improve the carrier transport within the type II scheme, semiconductor nanowires have already been used as the electron transporter in the inorganic–organic hybrid approach,[1–4] and recently an all-inorganic core/shell nanowire architecture has been proposed to improve both the electron and hole carrier transport and simultaneously the device stability, using well-known II–VI and III–V binary semiconductors, such as ZnO/ZnSe, ZnO/ZnTe, CdSe/CdTe, and GaN/GaP, and GaN/GaAs.[7,8] Here the type II transverse heterojunction functions similarly to a radial *p–n* junction[9,18] but without deliberate doping of the nanostructure. In addition, the type II core/shell structure may extend the absorption profile to a wavelength longer than that defined by the bandgap of any of the components through a relatively weak interface transition, as illustrated by the band diagram of ZnO/ZnSe in Figure 1.[7,8,19] When the core/shell nanowire is on the quantum mechanical scale, the ''interfacial'' absorption occurs between hole states more confined in one component and electron states more confined in the other component; thus, the absorption will be enhanced compared to the case when both components are on the mesoscopic scale.[7,8] Using highly lattice-mismatched combinations such as ZnO/ZnSe and GaN/GaP is more challenging in synthesis than less mismatched combinations such as CdSe/CdTe, but it offers more electronic structure tunability and better material stability.

In this Communication, we report success in synthesizing ZnO/ZnSe core/shell nanowires on a large-area, transparent, conducting substrate, using a relatively simple and low-cost approach combining chemical vapor deposition (CVD) and pulsed laser deposition (PLD). We have characterized their structural and optical properties by applying a comprehensive set of techniques. Although there have been many reports on vertically aligned single-component nanowire arrays or type I core/shell nanowire arrays on large substrates,[20–24] and there is also a report on nonvertically aligned GaN/GaP core/shell nanowires,[25] few efforts have been made to synthesize vertically aligned type II core/shell nanowire arrays, in particular using highly mismatched binaries. The successful achievement of this is a key step toward the demonstration of a new viable nanometer-scale solar cell technology.

A two-step synthesis was used to fabricate the ZnO/ZnSe core/shell nanowire array. First, a large-area (10 mm × 20 mm)

[*] Dr. W. L. Zhou, K. Wang, J. J. Chen
Advanced Materials Research Institute
University of New Orleans
New Orleans, LA 70148 (USA)
E-mail: wzhou@uno.edu
Dr. Y. Zhang, Dr. Y. F. Yan, Dr. J. Pern, Dr. A. Mascarenhas
National Renewable Energy Laboratory
Golden, CO 70148 (USA)
E-mail: yong_zhang@nrel.gov

[**] The work performed at UNO was supported by the DARPA grant no. HR0011-07-1-0032 through the AMRI and Louisiana Board of Regents contract no. LEQSF (2008-11)-RD-B-10. The work at NREL was supported by NREL LDRD and U.S. DOE/OS/BES, under contract no. DE-AC36-99GO10337. Supporting Information is available online from Wiley InterScience or from the authors.

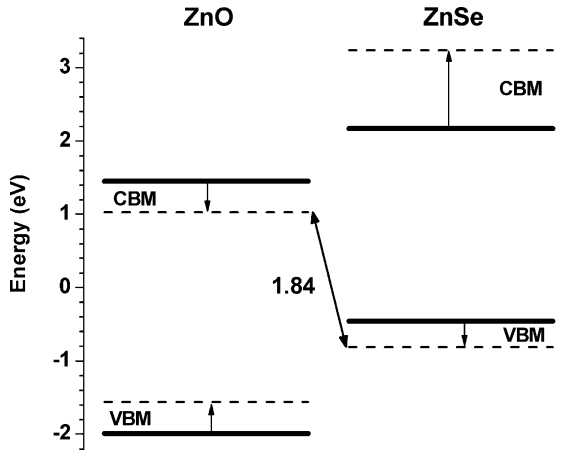

Figure 1. Energy diagrams of the bulk semiconductors ZnO and ZnSe at their natural lattice constants (solid lines) and the average lattice constant (dashed lines). CBM: conduction band minimum. VBM: valence band maximum. $E_g = 1.84$ eV is the estimated spatially indirect bandgap for a planar heterostructure.

well-aligned ZnO nanowire array, serving as the core for further deposition of the ZnSe shell, was synthesized directly on a transparent conducting oxide (TCO) substrate using CVD (see Fig. S1 in the Supporting Information). The experimental setup is similar to that of our previous work.[26] Subsequently, the TCO substrate with the ZnO nanowire array was transferred to the hot-wall PLD chamber, where PLD of ZnSe was carried out. In order to investigate the influence of deposition temperature on the crystallization of the ZnSe shell, room-temperature PLD of the ZnSe shell coating was also performed. In the PLD process, the thickness of the shell could be controlled by the target-to-substrate distance, deposition duration, pulse repetition frequency, and laser energy density.

Figure 2a shows a typical scanning electron microscopy (SEM) image of an as-synthesized ZnO nanowire array, presenting a uniform perpendicular growth of ZnO nanowires on the TCO substrate with an average length of 10 μm and diameters of 80–120 nm. After the PLD and followed annealing, the final nanowires, as shown in Figure 2b, exhibited increased wire diameters and rough surfaces, indicating that ZnSe was successfully deposited on the ZnO nanowires. The insets in Figures 2a and b are enlarged images of ZnO nanowire tips and a core/shell nanowire tip, respectively.

The X-ray diffraction (XRD) patterns of the ZnO nanowire array and the ZnO/ZnSe nanowire array are shown in Figure 3. The predominant ZnO peak from (002) planes indicates that the ZnO nanowires were grown with a *c*-axis orientation normal to the substrate surface. No characteristic diffraction peak of ZnSe was observed in the XRD pattern of the ZnO/ZnSe nanowire array because the ZnSe layer was very thin. By comparing the positions of the (100), (002), and (101) peaks of ZnO wurtzite (WZ) phase, it is seen that all peaks shift slightly to the smaller angle side after being coated with the ZnSe layer, which suggests that the ZnO lattice was enlarged. The shift

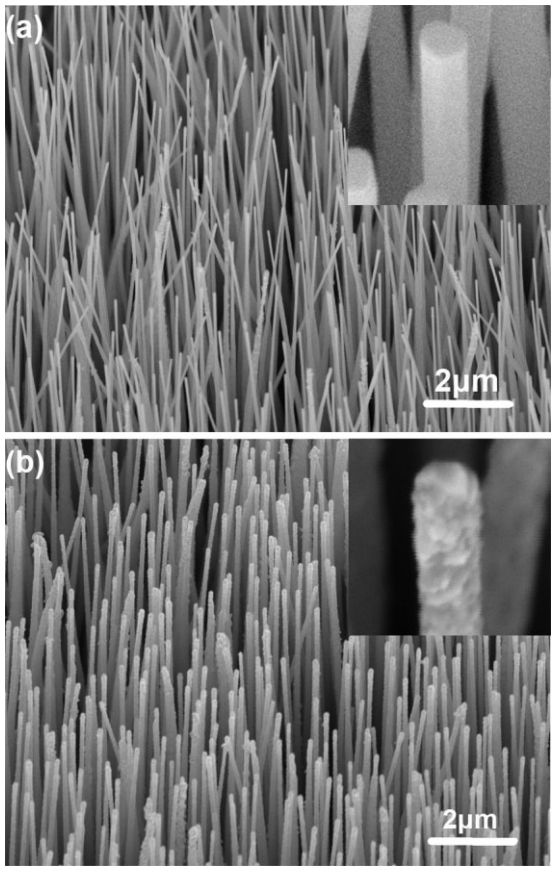

Figure 2. a) SEM image of a well-aligned ZnO nanowire array grown on a TCO substrate by CVD. The average length of the nanowires is about 10 μm and the diameters are about 100 nm. b) SEM image of well-aligned ZnO/ZnSe core/shell nanowire array prepared by PLD. The insets in (a) and (b) are enlarged images of ZnO nanowire tips and a core/shell nanowire tip, respectively.

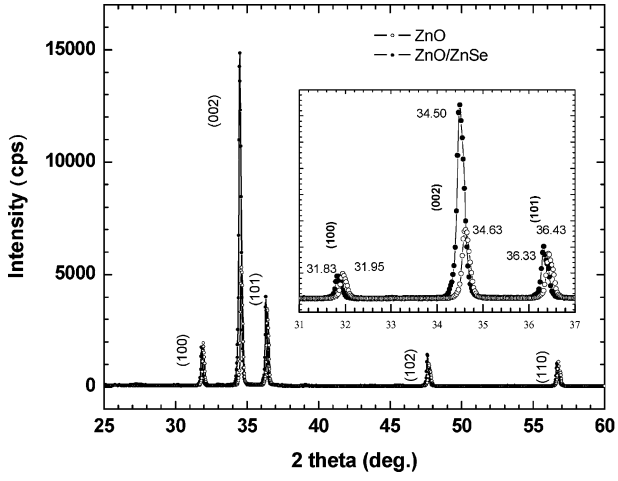

Figure 3. XRD patterns of ZnO and ZnO/ZnSe nanowire arrays. The inset shows a clear shift of the peaks to the smaller-angle side on going from ZnO to ZnO/ZnSe.

ADVANCED MATERIALS

might be attributed to the lattice expansion induced by the ZnSe shell growth, which will be discussed in more detail later.

The microstructures of the coated nanowires were further investigated using field emission transmission electron microscopy (TEM) and X-ray energy dispersive spectroscopy (EDS). Figure 4a shows a low-magnification TEM image of a ZnO/ZnSe core/shell nanowire with a rough external surface, but a sharp interface between the core and shell. The ZnSe shell grows directly in the radial direction from the surface of ZnO nanowire with a thickness of 5–8 nm. A high-resolution TEM image of the interface region between the ZnO core and ZnSe shell (marked by the rectangle in Fig. 4a), shown in Figure 4b, reveals that ZnO and ZnSe are of WZ and zinc blende (ZB) crystal structures, respectively. At the interface, an epitaxial growth of ZnSe from the ZnO core is observed. The interface is smooth and no transitional layer is found in between. The axis of the ZnO nanowire is identified to be the WZ *c*-axis. The epitaxial growth relationship of the WZ ZnO core and ZB ZnSe shell has been identified as $[0001]_{ZnO}//[001]_{ZnSe}$ and $(2\bar{1}\bar{1}0)_{ZnO}//(011)_{ZnSe}$. Figures 4c and d are the fast Fourier transform (FFT) patterns of the ZnO core and the ZnSe shell, indexed as WZ and ZB structures with zone axes $[2\bar{1}\bar{1}0]$ and [011], respectively, which also confirms the above epitaxial growth relationship. Defects were also observed in the interface along the *c*-axis of ZnO due to the large lattice mismatch, 8.8% along the nanowire axis between $c = 0.521$ nm for ZnO and $a = 0.567$ nm for ZnSe. Note that the lattice mismatch along the nanowire axis would be much larger (ca. 25%) if ZnO and ZnSe were both WZ phase. The spatial distributions of the atomic composition across the ZnO/ZnSe core/shell nanowire were obtained by a nanoprobe EDS line-scan analysis (marked by a line in Fig. 4a), showing that the ZnO nanowire was homogeneously coated, as shown in Figure 4e. It is also found that epitaxial growth only occurred during high-temperature deposition and no epitaxial growth was found for room-temperature deposition (shown in the Supporting Information, Fig. S2), indicating that the epitaxial growth between ZnO and ZnSe demands favorable thermodynamic as well as kinetic conditions. In the case of deposition performed at room temperature, the initial atoms being deposited do not gain enough migration energy from the system and condense at the very sites they arrive at on the surface of ZnO. They then aggregate with the next atoms to be deposited, forming a thick layer of polycrystalline ZnSe.

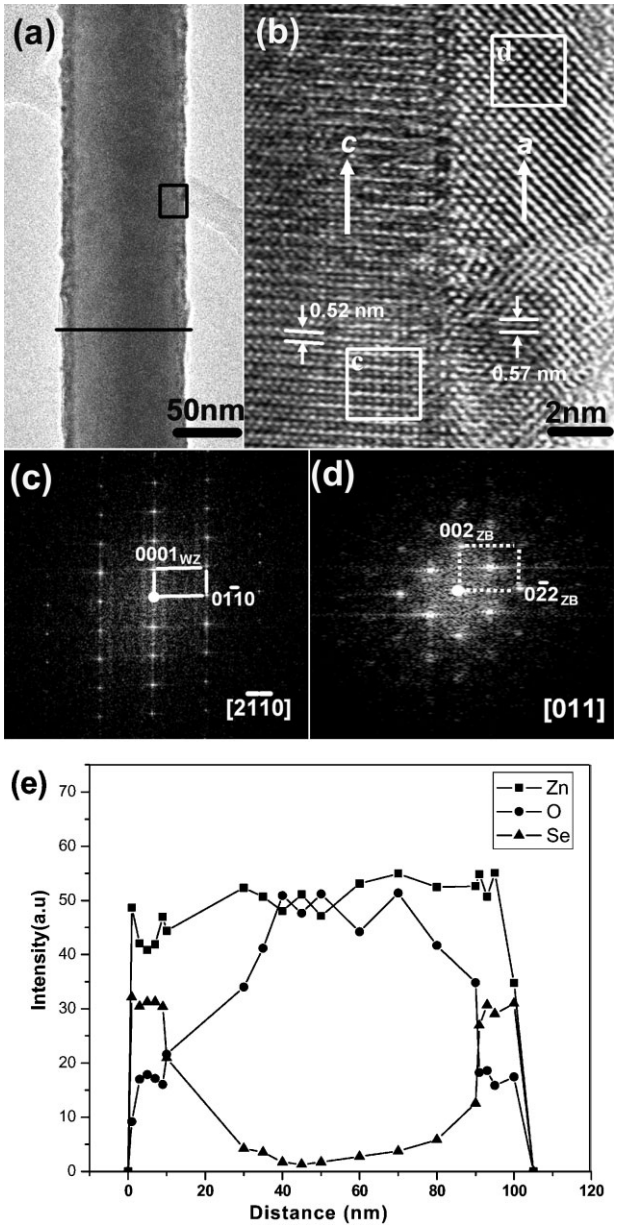

Figure 4. a) Low-magnification TEM image of a ZnO/ZnSe core/shell nanowire. A thin layer of ZnSe was coated on the ZnO nanowire. b) High-resolution TEM image of the interface of the core/shell heterostructure, enlarged from the rectangular area outlined in (a), showing the epitaxial growth relationship of the ZnO WZ core and ZnSe ZB shell. c,d) FFT patterns of the rectangular areas outlined in (b). e) EDS nanoprobe line-scan of the elements Zn, Se, and O, across the ZnO/ZnSe core/shell nanowire as indicated by the line in (a).

The optical properties of the ZnO/ZnSe core/shell nanowires were investigated by transmission, photoluminescence, Raman, and photoresponse measurements. Figure 5 shows typical transmission spectra of bare ZnO nanowires and ZnO/ZnSe core/shell nanowires. For the latter, two excitonic absorption peaks are clearly observed at the respective excitonic bandgaps (3.31 eV for WZ ZnO and 2.70 eV for ZB ZnSe), indicating good crystallinity of both core and shell. Similar to the cases of type II core/shell nanocrystals,[16,27] an additional absorption is found extending below the ZnSe bandgap into the near infrared. The component below the ZnSe bandgap could arise from a spatially indirect or an interfacial transition coupling a hole state in the ZnSe shell with an electron state in the ZnO core.

Figure 6a shows the PL spectra of ZnO and ZnO/ZnSe core/shell nanowires, compared with the spectrum of a high quality bulk *c*-plane ZnO single crystal purchased from Tokyo Denpa, Ltd. The reference sample shows bright emission visible to the

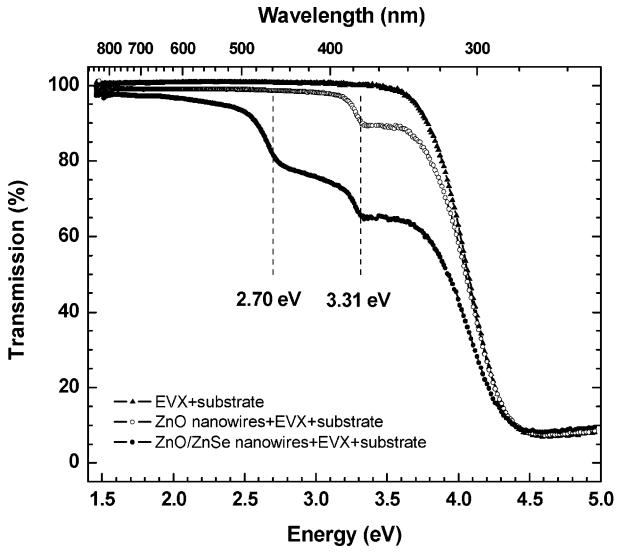

Figure 5. Transmission spectra of ZnO nanowires and the corresponding ZnO/ZnSe core/shell nanowires. The two vertical lines indicate the excitonic bandgaps of bulk ZnO and ZnSe. EVX: ethylene–vinyl acetate copolymer.

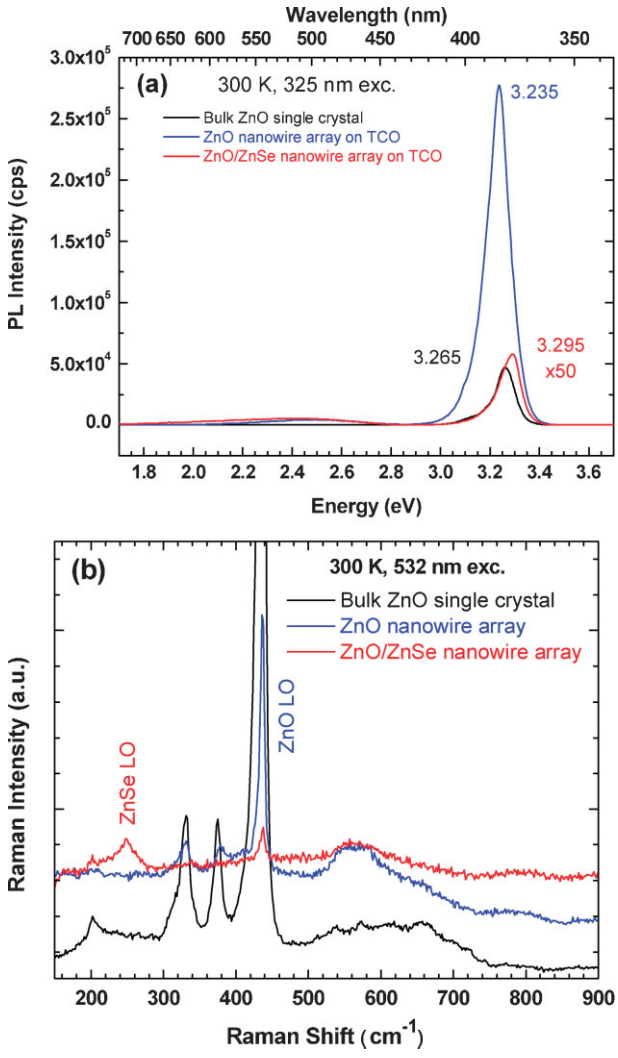

Figure 6. a) Photoluminescence and b) Raman spectra of ZnO and ZnO/ZnSe nanowire arrays, compared with those of a bulk ZnO single crystal.

naked eye upon excitation with a ca. 5 mW 325 nm laser: bandgap excitonic emission at 3.265 eV and a weak defect-related emission band at ca. 2.4 eV of ca. 0.5% of the band edge peak. Even without any intentional surface passivation of the bare ZnO nanowire array, the PL peak (at 3.235 eV) near the band edge of ZnO is found to be very strong, surprisingly, even exceeding that of the ZnO single crystal reference (which shows the strongest band edge emission among the several bulk ZnO samples tested) under nominally the same measurement conditions. Additionally, the ZnO nanowire array also shows a weak visible emission band (at ca. 2.49 eV, ca. 1.5% of the band edge peak). On one hand, the high PL intensity indicates the high interior crystal quality of the nanowires; on the other hand, two photonic-crystal-related effects might contribute to the high external quantum efficiency: 1) the waveguiding effect of the nanowire eliminates the lateral propagation,[28] and 2) a smaller effective dielectric constant of the array, as a result of averaging between the ZnO and air, than the bulk ZnO facilitates the escape of light from the sample. However, it is not entirely clear why the large surface area of the nanowires, and thus the expected large number of surface defects, does not seem to have a detrimental effect on the carrier recombination. For the core/shell nanowire array, the band edge emission remains strong but shifted to 3.295 eV, although reduced by roughly a factor of 300 from that of the bare ZnO nanowire array or ca. 50 from that of the bulk ZnO reference. There could be several possible reasons for the reduction: 1) charge separation between the core and shell (namely the hole relaxes into the shell but the electron remains in the core), 2) nonradiative recombination at possible defect sites of the core/shell interface, and 3) the absorption of the excitation and emission photons in the shell. Although the ZnSe shell is relatively thin and the absorption of a single path is relatively small (ca. 5% per 10 nm), multiple scattering in the nanowire array could significantly increase the absorption. Further investigation of the carrier dynamics associated with the core/shell interface and growth optimization are definitely needed, but we can at least conclude that the interface defects are not as detrimental as one might expect for such a highly mismatched heterostructure. No clearly identifiable emission is found from the shell, which is understandable giving the fact that the bandgap energy of the ZnSe shell overlaps with that of the defect band of the ZnO, that is, the ZnSe emission, if any, will be obscured, and also the ZnSe shell is relatively thin. However, for the core/shell nanowire array, a Raman peak of the ZnSe LO phonon at 248 cm^{-1}, as shown in Figure 6b, is observed in addition to the Raman features of ZnO (e.g., E_2 mode at 438 cm^{-1}), indicating that the ZnSe shell is crystalline or polycrystalline.

ADVANCED MATERIALS

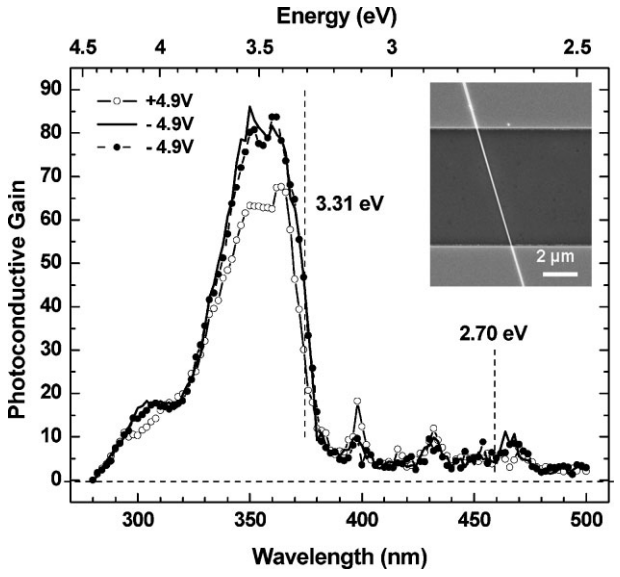

Figure 7. Photoconductivity spectra of a single ZnO/ZnSe nanowire measured under different biases and on different days. Inset: SEM image of the single-nanowire device for photoresponse measurements.

Photoresponse measurements were performed on a very preliminary device: a single core/shell nanowire resting on two Au electrodes at its two ends. Since the contacts are symmetric, the device is not expected to function as a single nanowire solar cell,[9] and a bias is needed to generate the photocurrent. Figure 7 shows the photoresponse spectra under positive and negative bias (switching the polarity of the bias voltage). A standard procedure for solar cell quantum efficiency measurement was followed, but with a bias, that is, the result should be considered as photoconductivity gain. Despite the photocurrent being rather small (a few picoamperes maximum), and the gain being significantly smaller than what has been reported previously for pure ZnO nanowires with more robust contacts,[29] the result is repeatable, stable, and perhaps more significantly the response shows an extension to the wavelength region below that of the ZnO bandgap. The existence of photoconductivity in the ZnSe spectral region indicates that the carriers are not fully depleted by defects at either the ZnO/ZnSe interface or the ZnSe surface, despite the ZnSe shell being fairly thin.

In summary, large-area, well-aligned, air-stable ZnO/ZnSe core/shell nanowire arrays were fabricated directly on TCO substrates by combining CVD and PLD, and their structures and optical properties were investigated in detail. SEM and TEM studies showed that the ZnO nanowires were uniformly and perpendicularly grown on the TCO substrate and the ZnSe shell with a thickness of 5–8 nm was epitaxially grown on the ZnO nanowire core. Absorption and photoconductivity studies show an extension of photoresponse into the region well below the ZnO bandgap. Such a core/shell nanowire array represents a novel architecture that could lead to a stable and efficient as well as low-cost solar cell technology for solar energy harvesting.

Experimental

Synthesis of ZnO Nanowire Arrays: To synthesize a large-area ZnO nanowire array, a piece of thin zinc foil was used to generate high pressure zinc vapor in a tube furnace. The Zn foil and TCO substrate were sequentially placed at a distance of 5 mm in a ceramic boat, which was then transferred to the center of a 2 in. (ca. 5 cm) diameter quartz tube furnace. The quartz tube was first evacuated to 10 mTorr (1 Torr = 133 Pa), and a 40 sccm (standard cubic centimeters per minute) argon flow was introduced into the tube, which was then heated to 600 °C at a rate of 30 °C min^{-1}. When the temperature exceeded 420 °C (the melting point of Zn), a 70 sccm air flow was also introduced into the quartz tube. The reaction was maintained for 30 min after the temperature reached 600 °C. By controlling the pumping rate, the pressure was kept at 8 Torr throughout the nanowire synthesis. The tube furnace was allowed to cool down naturally to room temperature in three hours. A white-yellowish layer was then obtained on the TCO substrate.

Synthesis of ZnO/ZnSe Nanowire Arrays: The as-synthesized ZnO nanowires, to be used as a template, were then transferred to the PLD chamber for ZnSe coating. A neodymium-doped yttrium aluminum garnet (Nd:YAG) laser was used to ablate the ZnSe disc target. The laser wavelength, energy density, and pulse frequency were 266 nm, 130 mJ cm^{-2}, and 2 Hz, respectively. The distance from the target to the TCO substrate with the ZnO nanowire array was 5 cm. Before the deposition, the vacuum system was first evacuated to 1×10^{-3} Torr. After the deposition had been performed at 400 °C for 20 min, the sample was annealed at 500 °C for 1 h. The room-temperature PLD for ZnSe shell coating was also performed in the same system at 27 °C for 20 min without any further annealing.

Characterization and Measurements: A Philips X'Pert-MPD X-ray diffractometer, a Carl Zeiss 1530 VP field emission scanning electron microscope, and a FEI Tecnai F20-UT high-resolution transmission electron microscope equipped with a nanoprobe energy-dispersive X-ray spectroscope were used to characterize the structure, morphology, and composition of the nanowires. The transmittance measurements were performed on a Varian Cary 5G UV-vis-NIR spectrophotometer with an integrating sphere (Labsphere DRA-CA-50), which enabled the results to be corrected for reflection and scattering losses. The nanowires were carefully scraped off the substrates with a blade, dispersed in a dilute toluene solution of ethylene–vinyl acetate copolymer (Elvax 150 or EVX, DuPont), then pipetted onto a microscope slide, and finally air-dried. A blank control was also prepared for reference. PL measurements were carried out at room temperature by using a setup consisting of a SPEX 1403 0.85 m double-grating spectrometer and a cooled RCA C31034 GaAs photomultiplier tube. The 325 nm line (ca. 5 mW) of a He-Cd laser was used for excitation, 50 μm slits were used. Raman measurements were performed on the same setup but a 532 nm laser with ca. 100 mW power was used instead, and 300 μm slits were used. To fabricate the device for photoresponse measurement, Au interdigital electrodes were first defined by electron-beam lithography on n-type degenerately doped silicon substrates with a 600 nm thermal oxide layer. The ZnO/ZnSe core/shell nanowires were scratched from the TCO substrate and spread into isopropyl alcohol (IPA) by ultrasonication. The nanowire solution was dispersed onto the silicon substrate by spin-coating at 200 rpm. By using a solution with the appropriate nanowire concentration, we were able to obtain and identify individual nanowires lying across two interdigital electrodes. The leads were added to the electrodes at locations away from the nanowire/electrode contacts. The photoresponse measurement was performed on a general-purpose broadband spectroscopy system consisting of a 100 W tungsten lamp, ISA Triax Series 320 spectrometer, Stanford

Research Systems SR570 current-preamplifier, and SR30DSP lock-in amplifier. The spectra were calibrated against a reference Si solar cell with a known quantum efficiency curve and for the ratio of the light spot size (ca. 2 mm × 4 mm) to the nanowire cross section (ca. 8 μm length × 110 nm diameter). The sensitivity of the measurement system is ca. 0.5 pA.

Received: January 15, 2008
Revised: March 9, 2008
Published online: July 14, 2008

[1] M. Adachi, Y. Murata, J. Takao, J. T. Jiu, M. Sakamoto, F. M. Wang, *J. Am. Chem. Soc.* **2004**, *126*, 14943.
[2] J. B. Baxter, E. S. Aydil, *Appl. Phys. Lett.* **2005**, *86*, 053144.
[3] M. Law, L. E. Greene, J. C. Johnson, R. Saykally, P. D. Yang, *Nat. Mater.* **2005**, *4*, 455.
[4] Y. M. Kang, N. G. Park, D. Kim, *Appl. Phys. Lett.* **2005**, *86*, 113101.
[5] Q. Shen, K. Katayama, T. Sawada, M. Yamaguchi, T. Toyoda, *Jpn. J. Appl. Phys.* **2006**, *45*, 5569.
[6] K. S. Leschkies, D. Ramachandran, J. Basu, E. Enache-Pommer, J. E. C. Boercker, B. Carter, U. R. Kortshagen, D. J. Norris, E. S. Aydil, *Nano Lett.* **2007**, *7*, 1793.
[7] Y. Zhang, L. W. Wang, A. Mascrenhas, *Nano Lett.* **2007**, *7*, 1264.
[8] J. Schrier, D. O. Demchenko, L. W. Wang, A. P. Alivisatos, *Nano Lett.* **2007**, *7*, 2377.
[9] B. Tian, X. Zheng, T. J. Kempa, Y. Fang, N. F. Yu, G. H. Yu, J. L. Huang, C. M. Lieber, *Nature* **2007**, *449*, 885.
[10] Y. Zhang, M. D. Sturge, K. Kash, B. P. van der Gaaq, A. S. Gozdz, L. T. Florez, J. P. Harbison, *Phys. Rev. B* **1995**, *51*, 13303.
[11] Y. Li, F. Qian, J. Xiang, C. M. Lieber, *Mater. Today* **2006**, *9*, 18.
[12] E. Yablonovitch, *Phys. Rev. Lett.* **1987**, *58*, 2059.
[13] M. Grätzel, *Nature* **2001**, *414*, 338.
[14] I. Robel, V. Subramanian, M. Kuno, P. V. Kamat, *J. Am. Chem. Soc.* **2006**, *128*, 2385.
[15] P. Yu, K. Zhu, A. G. Norman, S. Ferrere, A. J. Frank, A. J. Nozik, *J. Phys. Chem. B* **2006**, *110*, 25451.
[16] W. U. Huynh, J. J. Dittmer, A. P. Alivisatos, *Science* **2002**, *295*, 2425.
[17] I. Gur, N. A. Fromer, M. L. Geier, A. P. Alivisatos, *Science* **2005**, *310*, 462.
[18] B. M. Kayes, H. A. Atwater, N. S. Lewis, *J. Appl. Phys.* **2005**, *97*, 114302.
[19] S. Kim, B. Fisher, H. J. Eisler, M. Bawendi, *J. Am. Chem. Soc.* **2003**, *125*, 11466.
[20] L. E. Greene, M. Law, J. Goldberger, F. Kim, J. C. Johnson, Y. F. Zhang, R. J. Saykally, P. D. Yang, *Angew. Chem. Int. Ed.* **2003**, *42*, 3031.
[21] B. Xiang, Y. Zhang, Z. Wang, X. H. Luo, Y. W. Zhu, H. Z. Zhang, D. P. Yu, *J. Phys. D: Appl. Phys.* **2005**, *38*, 1152.
[22] A. P. Goodey, S. E. Eichfeld, E. E. Lew, J. M. Redwing, T. E. Mallouk, *J. Am. Chem. Soc.* **2007**, *129*, 12344.
[23] M. Law, L. E. Green, A. Radenovic, T. Kuykendall, J. Liphardt, P. D. Yang, *J. Phys. Chem. B* **2006**, *1101*, 22652.
[24] J. Noborisaka, J. Motohisa, S. Hara, T. Fukui, *Appl. Phys. Lett.* **2005**, *87*, 093109.
[25] H. M. Lin, Y. L. Chen, J. Yang, Y. C. Liu, K. M. Yin, J. J. Kai, F. R. Chen, L. C. Chen, Y. F. Chen, C. C. Chen, *Nano Lett.* **2003**, *3*, 537.
[26] J. J. Liu, M. H. Yu, W. L. Zhou, *Appl. Phys. Lett.* **2005**, *87*, 172505.
[27] S. A. Ivanov, A. Piryatinski, J. Nanda, S. Tretiak, K. R. Zavadil, W. O. Wallace, D. Werder, V. I. Klimov, *J. Am. Chem. Soc.* **2007**, *129*, 11708.
[28] M. Law, D. J. Sirbuly, J. C. Johnson, J. Goldberger, R. J. Saykally, P. D. Yang, *Science* **2004**, *305*, 1269.
[29] C. Soci, A. Zhang, B. Xiang, S. A. Dayeh, D. P. R. Aplin, J. Park, X. Y. Bao, Y. H. Lo, D. Wang, *Nano Lett.* **2007**, *7*, 1003.